Episodic Neoglacial expansion and rapid 20th Century retreat of a small ice cap on Baffin Island, Arctic Canada and modeled temperature change

5 Simon L. Pendleton[1], Gifford H. Miller[1], Robert A. Anderson[1], Sarah E. Crump[1], Yafang Zhong[2], Alexanda Jahn[3], Áslaug Geirsdottir[4]

[1]INSTAAR and Department of Geological Sciences, University of Colorado, Boulder, CO 80309-0450, USA.
[2]Space Science and Engineering Center, University of Wisconsin-Madison, Madison, WI 53706, USA.
10 [3]INSTAAR and Department of Atmospheric and Oceanic Sciences University of Colorado, Boulder, CO 80309-0450, USA.
[4]Department of Earth Sciences, University of Iceland, Askja, Sturlugata 7, 101 Reykjavík, Iceland

Correspondence to: Simon L. Pendleton (simon.pendleton@colorado.edu)

Abstract. Records of Neoglacial glacier activity in the Arctic constructed from moraines are often incomplete due to a
15 preservation bias toward the most extensive advance, usually the Little Ice Age. Recent warming in the Arctic has caused extensive retreat of glaciers over the past several decades, exposing preserved landscapes complete with *in situ* tundra plants previously entombed by ice. The radiocarbon ages of these plants define the timing of snowline depression and glacier advance across the site, in response to local summer cooling. Although most dead plants recently exposed by ice retreat are rapidly removed from the landscape by erosion, where erosive processes are unusually weak, dead plants may remain
20 preserved on the landscape for decades. In such settings, a transect of plant radiocarbon ages can be used to construct a near-continuous chronology of past ice margin advance. Here we present radiocarbon dates from the first such transect on Baffin Island, which directly dates the advance of a small ice cap over the past two millennia. The nature of ice expansion between 20 BCE and ~1000 CE is still uncertain, but episodic advances at ~1000, ~1200, and ~1500 CE led to the maximum Neoglacial dimensions ~1900 CE. We employ a two-dimensional numerical glacier model to reconstruct the pattern of ice
25 expansion inferred from the radiocarbon ages and to explore the sensitivity of the ice cap to temperature change. Model experiments show that at least ~0.44°C of cooling over the past 2 ka is required for the ice cap to reach its 1900 margin, and that the period from ~1000 to 1900 CE must have been at least 0.25°C cooler than the previous millennium; results that agree with regional climate model simulations. However, ~3°C of warming since 1900 CE is required to explain retreat to its present position, and, at the same rate of warming, the ice cap will disappear before 2100 CE.

30

1. Introduction

Although summer insolation in the Northern Hemisphere has declined steadily through the Holocene, favoring cryosphere expansion, glaciers worldwide are currently losing mass (Stocker et al., 2013). Globally, summer temperatures have been increasing over the last 60 years, a trend that is more pronounced at high latitudes due to strong positive feedbacks (Serreze

5   and Barry, 2011). Since summer temperatures are the dominant control on glacier mass balance in the Canadian Arctic (Koerner, 2005), the reversal of late Holocene cooling (Kaufman et al., 2009) has caused recent retreat of ice caps and glaciers in the region. This continued shrinkage of the cryosphere reinforces the need for records of past glacier and climate change to provide context for contemporary warming.

Patterns of Neoglacial advance and retreat in the Arctic remain poorly constrained (Solomina et al., 2015, and references

10   therein), largely because the most recent advance, during the Little Ice Age (LIA; 1250-1850 CE), was for most of the Arctic also the most extensive, and therefore obliterated most evidence of previous advances. Lake sediment records provide continuous records of climate, but typically allow glacial activity to be inferred indirectly. 'Threshold' lakes record a glacier entering and exiting a well-defined catchment, but provide the timing of a glacier margin at a single point (Briner et al., 2010). Lichenometric surface exposure dating, often used on glacial landforms, provides relative age information, but

15   conversion to absolute exposure age has large uncertainties (e.g., Osborn et al., 2015; Rosenwinkel et al., 2015). Furthermore, even though significant advances have been made improving analytical measurements for cosmogenic radionuclide (CRN) exposure ages of moraine boulders, the technique can be compromised by issues of nuclide inheritance, post-depositional movement, and moraine degradation (Crump et al., *in review*). Consequently, moraines can be difficult to date precisely, and moraine records by nature are discontinuous.

20   Recent ice-margin retreat of cold-based ice caps on Baffin Island is exposing preserved landscapes. The radiocarbon ages of *in situ* plants on these preserved lands record the time when snowline lowering and/or ice advance covered the site, killing and entombing the plants beneath the glacier. Commonly, the re-exposure of dead plants leaves them highly susceptible to erosion, most often by meltwater flowing along the margins of cold-based ice, but also by blowing snow in winter. The ephemeral nature of these re-exposed dead plants means that their ages are representative of the most recent snowline

25   advance at that location; multiple exposures and burials are unlikely (Miller et al., 2013).

However, in certain topographic settings, where plant removal by meltwater has been inefficient, dead plants may remain for decades. A transect of dead plant radiocarbon ages perpendicular to receding ice margin can provide a more reliable and more continuous record of ice advance than is possible from moraine records (Miller et al., 2017). The occurrence of long-preserved ice-killed tundra plants under optimal circumstances hundreds of meters beyond retreating ice margins provides an

30   opportunity to derive near-continuous records of ice-margin advance through the Neoglacial period. Here we present a chronology of ice-margin advance from Divide Ice Cap (informal name), a small mountain ice cap in southeastern Baffin Island, derived from radiocarbon-dated dead plants, and utilize numerical modeling to estimate the changes in summer temperature required to reproduce the observed record of ice margin advance.

2. Neoglaciation in the Eastern Canadian Arctic

There is substantial evidence of repeated glacier advances on Baffin Island during Neoglaciation (~5 ka through Little Ice Age; Miller et al., 2005) as summer temperatures declined, but absolute chronologies remain sparse and imprecise. Foundational mapping and initial chronologies derived from lichenometry from nested moraines show that some glaciers

5   were approaching their Neoglacial maximum dimensions as early as 3.5 ka (Davis, 1985; Miller, 1973). Radiocarbon ages of tundra plants killed by snowline depression, and only now re-emerging from beneath cold-based ice, show that glaciers began to expand as early as ~5 ka, followed by episodic intensifications culminating in the Little Ice age (Anderson et al., 2008; Miller et al., 2012; 2013; Margreth et al., 2014). Although most studies conclude that glaciers reached their maximum Neoglacial dimensions during the LIA, Young et al. (2015) produced a CRN chronology of nested moraines in northeastern

10   Baffin Island that suggests that Naqsaq glacier advanced to a position similar to that of its LIA extent at ~1050 CE. However, moraine chronologies hinting at the nature of pre-LIA temperature change are sparse, and the chronology from an individual site can be influenced by non-climatic factors; thus, other datasets that provide direct evidence of Neoglacial ice advance are needed.

3. Field Setting: Divide Ice Cap

15   Divide Ice Cap (DIC) is situated ~60 km southwest of the settlement of Qikitarjuaq on eastern Baffin Island (Fig. 1). The ice cap currently mantles the northern slope of a local summit between ~1550 and 1180 m asl, spilling down into a local saddle, where it separates into two outlet glaciers flowing down either side of the saddle, orthogonal to the main ice cap flow. A vegetation trimline high on the south-facing slope on the opposite side of the saddle defines the maximum LIA limit (Fig. 1). Aerial imagery from 1960 show the ice margin ~15 m below this trimline (Fig. 1; National Air Photo Library, 1960).

20   The 2015 ice margin lies 60 m below the LIA trimline. Our sample transect runs from the modern ice margin upslope toward the LIA trimline and is aligned with the topographic drainage divide where ice growth upslope is driven by internal deformation (Fig. 2). Between the ice margin and the trimline, the land surface is carpeted by till boulders amidst finer-grained morainal debris. The presence of preserved plants still in growth position exposed by the retreating ice margin is evidence for a high degree of subglacial landscape preservation, indicating a cold-based, non-erosive basal regime for the

25   DIC at our transect.

Until now, the majority of studies utilizing dates on previously ice-entombed plants rely on plants collected close to the ice margin at multiple ice caps to build a composite dataset that highlights periods of regional cooling (e.g., Anderson et al., 2008; Miller et al., 2013; Margreth et al., 2014). However, because meltwater erosion at the location of our transect was inefficient, *in situ* dead plants remain preserved from the ice margin to the trimline, although with decreasing abundance at

30   higher elevations as the trimline is approached (Fig. 1). Miller et al. (2017) recently employed a similar method on Svalbard by collecting a transect of six, dead, *in situ* mosses up to 250 m away from the 2013 CE ice margin. The radiocarbon ages of these plants provide evidence of an episodically advancing ice margin over the last ~1200 years.

4. Methods

4.1. Vegetation Collection

In August 2015, when seasonal melt was at its maximum, 11 *in situ* dead mosses were collected along a ~200 m transect between the 2015 CE ice margin (1185 m asl) and the LIA trimline (1238 m asl) (Fig. 1). Within ~5 m of the ice margin, all

5 exposed vegetation was dead. Regrowth and recolonization of plants began ~30 m from the ice margin, with dead plants increasingly rare, and living plants increasingly abundant up the transect. During field collection, plants are closely inspected for spontaneous regrowth, which is discernable in the field based on plant color (La Farge et al., 2013). Woody plants were avoided because of their higher survival potential and because their stems have an average radiocarbon age that is older than the actual kill date. In the previous year, we collected *in situ* dead vegetation at the southern margin of the ice cap, closer to

10 the summit (1438 m asl; Fig. 1).

Between 1 and 3 filaments from each sampled plant were washed with deionized water and freeze dried before being graphitized at the Laboratory for AMS Radiocarbon Preparation and Research (NSRL). Graphite targets were measured at the W.M. Keck Carbon Cycle Accelerator Mass Spectrometry Laboratory at the University of California Irvine. Final radiocarbon dates were calibrated using OxCal 4.2.4 (Bronk-Ramsey, 2009; Reimer et al., 2013) and reported here as the

15 weighted mean, 1σ, and 2σ uncertainties.

4.2. Glacier Model

We employ a two-dimensional finite difference numerical model in conjunction with the *in situ* vegetation to further investigate the evolution of the Divide Ice Cap over the last ~2000 years. Here we briefly describe the model setup; for a detailed explanation see Supplemental information. The model, modified from Kessler et al. (2006), calculates an ice

20 thickness on a two-dimensional terrain model governed by explicit equations for ice flux and mass balance using shallow-ice physics (Blatter et al., 2011). Modern ice was removed (using an approximation of basal shear stress of ~1 bar) from 2011 ASTER digital elevation data to create the base terrain on which glacier growth was modeled.

Glacier growth on the base terrain was driven using a modified distributed mass-balance approach. Annual accumulation is assumed to be uniform (0.3 m water equivalent) across the ice cap, given the small area and limited elevation range (Fisher

25 et al., 1998; WGMS, 2012). Annual melt is calculated using a positive degree day method (Hock, 2005) with an additional component from incoming solar radiation (Jonsell et al., 2012). We apply a positive degree day melt factor of 6.3 mm day^{-1} °C^{-1} (Braithwaite, 1981). Solar radiation melt factors (mm day^{-1} (W m^{-2})$^{-1}$) are traditionally calibrated using measurements of mass balance (e.g., Jonsell et al., 2012); at this study site we lack such measurements. However, using the temporal and spatial constraints above, including the maximum Neoglacial ice configuration recorded by trimlines, the local solar

30 radiation melt factor can be approximated from the model run that produces the best-fit ice extent to the observed Neoglacial maximum extent.

5. Results and Interpretation

5.1. Plant Ages

The single *in situ* sample collected on the southern margin of DIC produced a calibrated age of 26 +29/-21 CE (Fig. 1, Table 1). Calibrated radiocarbon ages of plant material from the transect become younger away from DIC, ranging from 942 +41/-36 and 1029 +33/-3 CE at the 2015 ice margin to 1780 +111/-165 CE near the trimline. The ages of four samples closest to the 2015 ice margin, although collected up to ~20 m away from the margin, overlap at ±2σ (Table 1). A single plant collected near the LIA trimline returned a post-bomb age; as this likely reflects random death of a plant that recolonized after deglaciation (Fig. 1, Table 1), it is not included in the summary figures.

5.2. Neoglacial Divide Ice Cap Expansion and 20th Century recession

The kill date at the southern margin of DIC indicates ice expansion across that location ~2 ka and continuous ice-cover until 2014 CE. The transect ages track expansion of DIC beginning ~1000 CE (Fig. 3). The progressively younger ages upslope along the transect record the episodic advance of the ice margin by accretion and internal deformation, rather than sliding. The ages near the 2015 CE ice margin (henceforth the 1000 CE margin) define DIC expansion ~1000 CE. The remaining kill dates align with periods of enhanced regional cooling shown in the composite population of dated ice-entombed mosses from the Cumberland Peninsula region, centered on ~1000, 1200, and 1500 CE (Fig. 3; Anderson et al., 2008; Miller et al., 2013; Margreth et al., 2014; this study). Possible explanations for the discontinuities between moss dates include continued expansion, ice margin stasis, or ice recession. However, the spatial and temporal distribution of the transect data and their correspondence with regional ice-expansion records supports our interpretation that DIC expanded episodically between ~1000 and 1900 CE.

The proximity of the highest elevation radiocarbon sample to the trimline suggests that DIC approached its Neoglacial maximum position sometime between ~1600 CE and the end of the 19th century. Aerial photographs from 1960 show that the ice margin had already retreated ~15 m vertically from its maximum extent (trimline), indicating abandonment of its Neoglacial maximum position prior to 1960 (Fig. 1).

5.3. Ice Cap Modelling

Using the above spatial and temporal constraints on ice margin movement over the last ~2000 years, model simulations can be used to explore the climate sensitivity of the Divide Ice Cap system, and to estimate the temperature changes required to reproduce the observed advance and retreat cycle. A solar radiation melt factor of 0.036 mm day^{-1} (W m^{-2})$^{-1}$ produced the closest match to the Neoglacial maximum extent geometry (Supplement Fig. 3). Assuming a stable ice cap with a margin just inside sample 12, the model requires an average minimum summer cooling of 0.19°C persisting for 1000 years to grow ice across the southern sample location and reach the 1000 CE margin in the allotted ~1000 years. A subsequent additional cooling of ~0.25°C is required for ice to advance across the 1000 CE margin to the LIA trimline by 1900 CE. It is of course

likely that some decades were much colder than others; our modeling suggests that a minimum average cumulative summer cooling of ~0.44°C over the ~1900 years is required to advance the observed DIC ice margin through the constraints provided by the kill dates.

Building upon the ice expansion simulations, the model was used to investigate recent warming and ice retreat. DIC likely began receding around ~1900 CE, retreating from its maximum extent to its modern position over the past ~100 years. Under a simple linear warming scenario of 0.028°C yr^{-1}, the modeled DIC retreats from the LIA trimline to its 2015 position in 105 years. This rate of warming is slightly higher than the 0.014°C yr^{-1} (since 1959 CE) documented from the interior Dewar Lakes weather station ~320 km to the northwest, but significantly lower than the recent warming rate from Qikiqtarjuaq (0.87 °C yr^{-1} 1995-2009 CE). The modeled rate of warming amounts to ~2.8°C of cumulative warming over the last century, which is similar to values recorded elsewhere in the Eastern Canadian Arctic (Bekryaev et al., 2010; Stocker et al., 2013). Continuing under the same rate of warming, DIC will disappear by ~2100, and sooner if local warming accelerates.

The temperature changes reported here are minimum values due to assumptions made in the model. The best available data was used for both model initial conditions and mass balance forcings, but limitations in these data introduce significant uncertainty to the model (see Supplemental). However, the general agreement of ice cap simulations to observational data in the region support the first-order model results presented here.

6. Discussion

6.1. Regional Comparisons

The timing of episodes of ice expansion found here agrees well with those found by Miller et al. (2016) at ~1100 and 1500 CE, using a similar transect method in Svalbard. Also, similar to the Svalbard work, we find that DIC reached its maximum Neoglacial extent during the LIA and that warming since the early 1900s has reduced glacier dimensions to a smaller size than any time since 1000 CE.

The magnitude of Neoglacial glacier advances and derived climate interpretations presented here differ somewhat from those based on the Naqsaq valley moraine suite farther north on Baffin Island. Based on sets of tightly clustered [10]Be ages on moraines boulders in a nested moraine complex, Young et al. (2015) suggests that the Naqsaq glacier reached a position similar to that of its LIA extent at ~1050 CE. This led the authors to suggest that the climate was similar, with little or no additional cooling from ~1050 CE through the LIA. This interpretation differs from both the observed significant expansion of DIC from ~1000 CE to its LIA maximum, and the model simulations requiring that the same time period must have been, on average, ~0.25°C cooler than the preceding millennium.

This discrepancy between the two records may be explained by non-climatic factors affecting the deposition and preservation of moraines. Glaciers with a majority of their area at high elevations relative to the glacier tongue may not respond uniformly to equilibrium line altitude (ELA) fluctuations (e.g., Pedersen and Egholm, 2013). At the site studied by

Young et al. (2015), the majority of the glacier area resides on a high plateau, with a narrow outlet glacier occupying a deeply incised valley, terminating in an open, wide valley floor. Although the moraine chronology developed by Young et al. (2015) itself is strong, it is possible that the termimal position is relatively insensitive to small Late Holocene ELA changes. This is because once the ELA drops below the plateau and is within the narrow outlet glacier, each incremental ELA

5   lowering increases the accumulation area only slightly. In contrast, DIC has a more symmetric hypsometry (i.e., the glacierized area is more evenly distributed over glacier elevation). Consequently, we expect that the correlation between ELA change and glacier dimension response should be more linear than for Naqsaq Glacier. Both the plant radiocarbon dates and glacier model simulations require increased summer cooling between ~1000 CE and the LIA.

6.2. Climate model/glacier model comparisons

10 Recent climate simulation with an earth system model provides a test of our glacier-model derived estimate of temperature change over the past 2 ka. Here we make use of a new 0-1270 CE simulation with the Community Earth System Model (CESM) (Hurrell et al. 2013), which adopts the same model version of the CESM as used for the CESM – Last Millennium Ensemble (LME) (Otto-Bliesner et al., 2016) driven by natural (i.e. orbital parameters, solar irradiance, and volcanic eruptions) and anthropogenic forcings (i.e. greenhouse gases and land-use) compiled by the PMIP4 working group

15 (Jungclaus et al., 2016). When combined with years 850-1850 CE from the CESM LME ensemble member 12 (Otto-Bliesner et al., 2016), the composite simulation allows us to quantify the average cooling in the North Atlantic Arctic air temperature during JJA from 0-1850 CE. When combining the two simulations, we use their temperature difference during the overlap period to correct for a systematic temperature offset (see Supplemental information). The corrected and combined simulation suggests that the period from 0-1000 CE was, on average, ~0.24°C cooler than 1 CE control conditions

20 (Fig. 4), and that the period from 1000-1850 CE was on average ~0.30°C cooler than the preceding millennium, meaning that the period from 0-1850 CE was, on average, ~0.54°C cooler than 1 CE conditions, and that the second millennium CE temperature decline was dominated by cooling through the LIA (Fig. 4). The period encapsulating the LIA, from 1250-1850 CE, was on average 0.40°C cooler than 0-1000 CE. The climate model simulations are in agreement with the glacier-model derived summer temperature change estimates presented above, supporting our contention that the record of DIC expansion

25 derived from the death ages of entombed plants faithfully records the average cooling that occurred in the region over the past 2000 years.

7. Conclusions

We have used radiocarbon-dated *in situ* tundra plants exposed by retreating ice margins to construct a spatially and temporally constrained record of ice cap expansion over the past 2 ka. DIC grew between ~26 BCE and 1000 CE, then

30 advanced episodically at ~1000, 1200, and 1500 CE, reaching its Neoglacial maximum during the LIA. The LIA was terminated by warming of the 20th century.

Glacier model simulations show that a minimum average cooling of ~0.44°C is required to match the radiocarbon constrained pattern of ice expansion over the last 2000 years, with the period from 1000 to 1850 CE being on average ~0.25°C colder than the preceding ~1000 years. Climate model simulations for the past 2ka driven by natural and anthropogenic forcings show similar summer temperature decreases, reinforcing the glacier modeling conclusions. Both the

5   radiocarbon record and climate model simulations indicate that the coldest interval of the past ~2000 years was during the LIA (1250-1850 CE). Glacier model simulations matching observed ice-cap retreat since 1900 CE suggest that a cumulative warming of ~3°C over the last ~100 years has reversed ~1000 years of ice cap expansion under only ~0.25°C cooling, suggesting modern warming is unprecedented over the past 2 ka.

At the present rate of warming, DIC will likely disappear before ~2100. Future collection of *in situ* plants exposed as DIC

10   continues to retreat will both extend the record of ice cap advance and provide more constraint for modeling of ice cap activity and climate perturbations during Neoglaciation.

Acknowledgements.

The authors thank Nicolás Young for assistance in the field, Polar Continental Shelf Project and Universal Helicopters for logistical support, and the Inuit of Qikiqtarjuaq for permission to conduct research on their lands and field assistance. Scott

15   Lehman and John Southon provided radiocarbon analyses. This project was supported by NSF award ARC-1204096. Contributions of R.S.A. were supported by NSF award EAR-1548725. Climate Modeling was supported by RANNIS ANATILS award 141573-052 and NSF-PLR1418040. The CESM 1 CE and past2K simulations were performed on the high-performance supercomputer Yellowstone (ark:/85065/d7wd3xhc) provided by NCAR's Computational and Information Systems Laboratory, sponsored by the National Science Foundation.

20

References

Anderson, R. K., Miller, G. H., Briner, J. P., Lifton, N. A. and DeVogel, S. B.: A millennial perspective on Arctic warming from 14C in quartz and plants emerging from beneath ice caps, Geophys. Res. Lett., 35(1), 2008.

Bekryaev, R. V., Polyakov, I. V. and Alexeev, V. A.: Role of polar amplification in long-term surface air temperature

25   variations and modern arctic warming, J. Clim., 23(14), 3888–3906, doi:10.1175/2010JCLI3297.1, 2010.

Blatter, H., Greve, R. and Abe-Ouchi, A.: Present State and Prospects of Ice Sheet and Glacier Modelling, Surv. Geophys., 32(4–5), 555–583, doi:10.1007/s10712-011-9128-0, 2011.

Braithwaite, R. J.: On glacier energy balance, ablation, and air temperature., J. Glaciol., 27(97), 381–391, 1981.

Briner, J. P., Stewart, H. A. M., Young, N. E., Philipps, W. and Losee, S.: Using proglacial-threshold lakes to constrain

30   fluctuations of the Jakobshavn Isbr?? ice margin, western Greenland, during the Holocene, Quat. Sci. Rev., 29(27–28),

3861–3874, doi:10.1016/j.quascirev.2010.09.005, 2010.

Bronk-Ramsey, C.: Bayesian Analysis of Radiocarbon Dates, Radiocarbon, 51(1), 337–360, doi:10.2458/azu_js_rc.51.3494, 2009.

Crump, S. E., Anderson, L. S., Miller, G. H. and Anderson, R. S.: Interpreting exposure ages from ice-cored moraines: A

5 Neoglacial case study on Baffin Island, Arctic Canada, , in review, n.d.

Davis, P. T.: Neoglacial moraines on Baffin Island, Quat. Environ. East. Can. Arctic, Baffin Bay West. Greenland. Allen Unwin, Bost., 682–718, 1985.

La Farge, C., Williams, K. H. and England, J. H.: Regeneration of Little Ice Age bryophytes emerging from a polar glacier with implications of totipotency in extreme environments, Proc. Natl. Acad. Sci., 110(24), 9839–9844,

10 doi:10.1073/pnas.1304199110, 2013.

Fisher, D. A., Koerner, R. M., Bourgeois, J. C., Zielinski, G., Wake, C., Hammer, C. U., Clausen, H. B., Gundestrup, N., Johnsen, S. and Goto-Azuma, K.: Penny ice cap cores, Baffin Island, Canada, and the Wisconsinan Foxe Dome connection: Two states of Hudson Bay ice cover, Science (80-.)., 279(5351), 692–695, 1998.

Hock, R.: Glacier melt: a review of processes and their modelling, Prog. Phys. Geogr., 29(3), 362–391,

15 doi:10.1191/0309133305pp453ra, 2005.

Jonsell, U., Navarro Valero, F. J., Bañón, M., Izargain, L., Jesús, J. and Otero García, J.: Sensitivity of a distributed temperature-radiation index melt model based on AWS observations and surface energy balance fluxes, Hurd Peninsula glaciers, Livingston Island, Antarctica, Cryosph., 6(3), 539–552, 2012.

Kaufman, D. S., Schneider, D. P., McKay, N. P., Ammann, C. M., Bradley, R. S., Briffa, K. R., Miller, G. H., Otto-Bliesner,

20 B. L., Overpeck, J. T. and Vinther, B. M.: Recent warming reverses long-term arctic cooling., Science, 325(5945), 1236–9, doi:10.1126/science.1173983, 2009.

Kessler, M. A., Anderson, R. S. and Stock, G. M.: Modeling topographic and climatic control of east-west asymmetry in Sierra Nevada glacier length during the Last Glacial Maximum, J. Geophys. Res. Earth Surf., 111(2), 1–15, doi:10.1029/2005JF000365, 2006.

25 Margreth, A., Dyke, A. S., Gosse, J. C. and Telka, A. M.: Neoglacial ice expansion and late Holocene cold-based ice cap dynamics on Cumberland Peninsula, Baffin Island, Arctic Canada, Quat. Sci. Rev., 91, 242–256, doi:10.1016/j.quascirev.2014.02.005, 2014.

Miller, G. H.: Late Quaternary glacial and climatic history of northern Cumberland Peninsula, Baffin Island, N.W.T., Canada, Quat. Res., 3(4), 561–583, doi:http://dx.doi.org/10.1016/0033-5894(73)90031-8, 1973.

30 Miller, G. H., Wolfe, A. P., Briner, J. P., Sauer, P. E. and Nesje, A.: Holocene glaciation and climate evolution of Baffin Island, Arctic Canada, Quat. Sci. Rev., 24(14–15), 1703–1721, doi:10.1016/j.quascirev.2004.06.021, 2005.

Miller, G. H., Geirsdóttir, Á., Zhong, Y., Larsen, D. J., Otto-Bliesner, B. L., Holland, M. M., Bailey, D. A., Refsnider, K. A., Lehman, S. J. and Southon, J. R.: Abrupt onset of the Little Ice Age triggered by volcanism and sustained by sea-ice/ocean feedbacks, Geophys. Res. Lett., 39(2), 2012.

Miller, G. H., Lehman, S. J., Refsnider, K. A., Southon, J. R. and Zhong, Y.: Unprecedented recent summer warmth in Arctic Canada, Geophys. Res. Lett., 40(21), 5745–5751, 2013.

Miller, G. H., Landvik, J. Y., Lehman, S. J. and Southon, J. R.: Episodic Neoglacial snowline descent and glacier expansion on Svalbard reconstructed from the 14C ages of ice-entombed plants, Quat. Sci. Rev., 155, 67–78, doi:10.1016/j.quascirev.2016.10.023, 2017.

National Air Photo Library.: A17014. Photos: 83-84 Ottawa: Department of Energy, Mines and Resources, 1960.

Osborn, G., McCarthy, D., LaBrie, A. and Burke, R.: Lichenometric dating: Science or pseudo-science?, Quat. Res., 83(1), 1–12, 2015.

Otto-Bliesner, B. L., Brady, E. C., Fasullo, J., Jahn, A., Landrum, L., Stevenson, S., Rosenbloom, N., Mai, A. and Strand, G.: Climate variability and change since 850 ce an ensemble approach with the community earth system model, Bull. Am. Meteorol. Soc., 97(5), 787–801, doi:10.1175/BAMS-D-14-00233.1, 2016.

Pedersen, V. K. and Egholm, D. L.: Glaciations in response to climate variations preconditioned by evolving topography, Nature, 493(7431), 206–10, doi:10.1038/nature11786, 2013.

Reimer, P. J., Bard, E., Bayliss, A., Beck, J. W., Blackwell, P. G., Bronk Ramsey, C., Buck, C. E., Cheng, H., Edwards, R. L., Friedrich, M., Grootes, P. M., Guilderson, T. P., Haflidason, H., Hajdas, I., Hatté, C., Heaton, T. J., Hoffmann, D. L., Hogg, A. G., Hughen, K. A., Kaiser, K. F., Kromer, B., Manning, S. W., Niu, M., Reimer, R. W., Richards, D. A., Scott, E. M., Southon, J. R., Staff, R. A., Turney, C. S. M. and van der Plicht, J.: IntCal13 and Marine13 Radiocarbon Age Calibration Curves 0–50,000 Years cal BP, Radiocarbon, 55(4), 1869–1887, doi:10.2458/azu_js_rc.55.16947, 2013.

Rosenwinkel, S., Korup, O., Landgraf, A. and Dzhumabaeva, A.: Limits to lichenometry, Quat. Sci. Rev., 129, 229–238, doi:10.1016/j.quascirev.2015.10.031, 2015.

Serreze, M. C. and Barry, R. G.: Processes and impacts of Arctic amplification: A research synthesis, Glob. Planet. Change, 77(1–2), 85–96, doi:10.1016/j.gloplacha.2011.03.004, 2011.

Solomina, O. N., Bradley, R. S., Hodgson, D. A., Ivy-Ochs, S., Jomelli, V., Mackintosh, A. N., Nesje, A., Owen, L. A., Wanner, H., Wiles, G. C. and Young, N. E.: Holocene glacier fluctuations, Quat. Sci. Rev., 111, 9–34, doi:10.1016/j.quascirev.2014.11.018, 2015.

Stocker, T. F., Qin, D., Plattner, G.-K., Tignor, M., Allen, S. K., Boschung, J., Nauels, A., Xia, Y., Bex, V. and Midgley, P. M.: Climate change 2013: The physical science basis, Intergov. Panel Clim. Chang. Work. Gr. I Contrib. to IPCC Fifth Assess. Rep. (AR5)(Cambridge Univ Press. New York), 2013.

WGMS: Flucuations of Glaciers 2005–2010 (Vol. X), ICSU(WDS)/IUGG(IACS)/UNEP/UNESCO/WMO, World Galcier Monit. Serv. Zurich, Switz., X, 336, 2012.

Young, N. E., Schweinsberg, A. D., Briner, J. P. and Schaefer, J. M.: Glacier maxima in Baffin Bay during the Medieval Warm Period coeval with Norse settlement, , (December), doi:10.1126/sciadv.1500806, 2015.
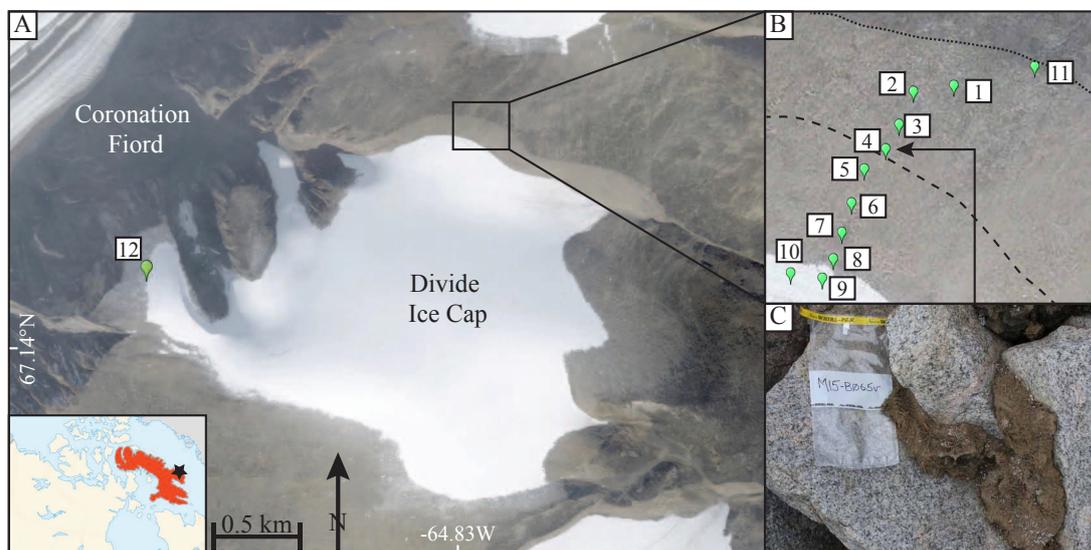
Figure 1: A) A map view of Divide Ice Cap, with location in inset map; note prominent trimlines and location of sample #12. B) Detail of sampling transect along which mosses were collected (sample numbers noted), with trimline (dotted line) and 1960 ice margin (dashed line; based on aerial photographs) shown. C) Example of sampled in situ preserved moss along transect (sample #5).
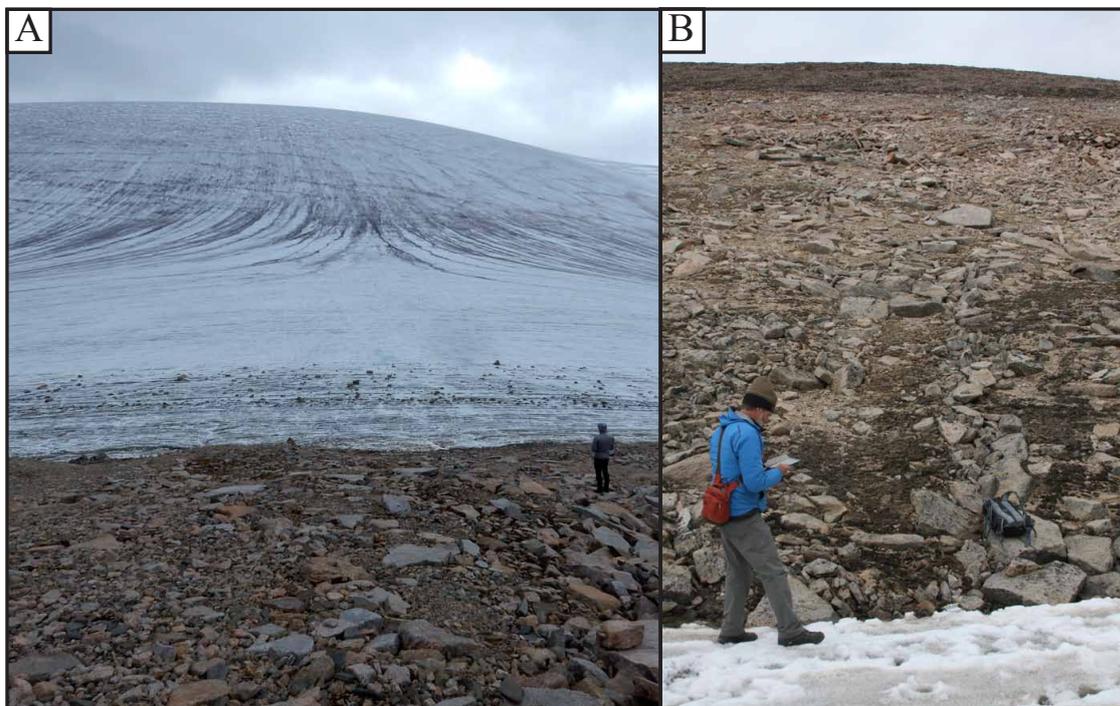
Figure 2: A) View south towards north aspect of DIC, with supraglacial channels demarcating the modern topographic divide. B) View north along transect up towards the maximum Neoglacial DIC extent; note large mats of dead vegetation diminish away from current ice margin.
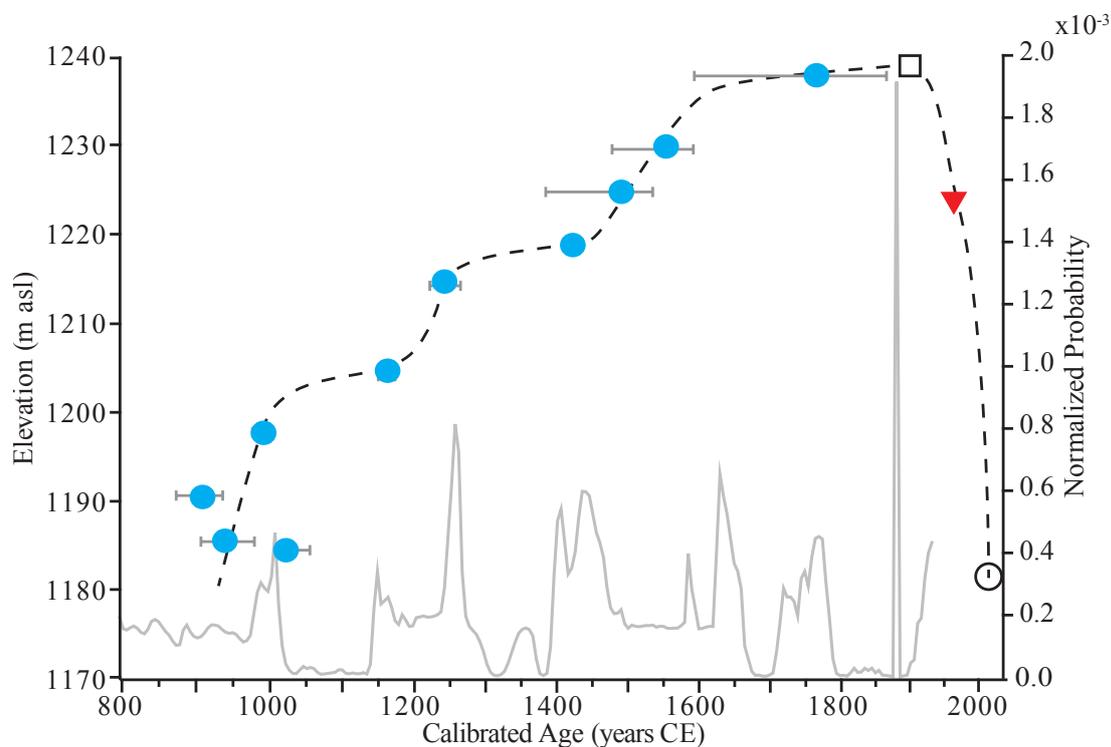
Figure 3: Plot of transect radiocarbon ages with elevation, showing median age (dots) and 1-sima uncertainty (gray bars). Position of ~1900 CE Neoglacial maximum extent (square) also shown. The position of the DIC margin interpreted from 1960 aerial photographs is shown (triangle), as well as its observed 2015 position (circle). Also plotted is the aggregate normalized yearly probability for dated *in situ* plant samples in the Cumberland Peninsula region (gray line; *n=70*), including those from Miller et al. (2013) and Margreth et al. (2014). The inferred ice margin history (dashed line) plotted through samples ages illustrates the episodic nature of ice margin advance.
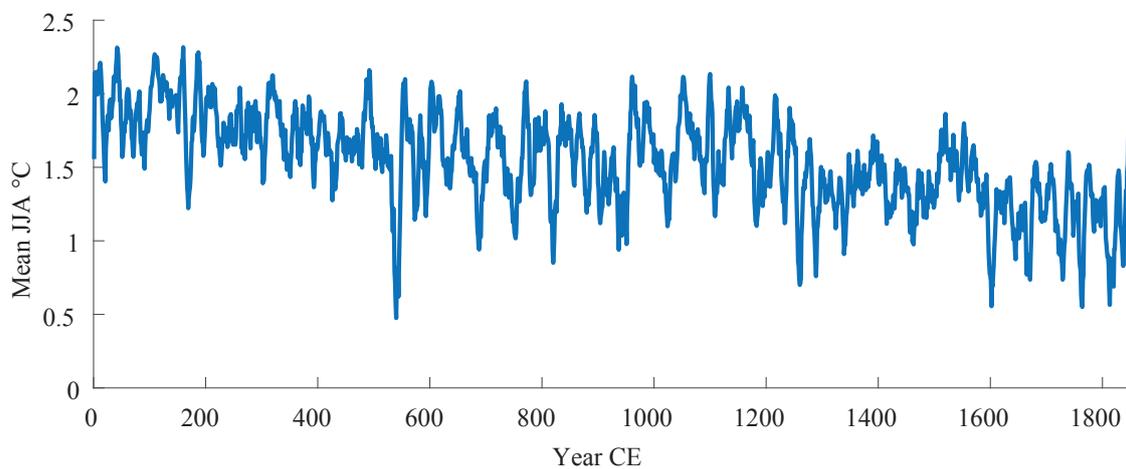
Figure 4: ESM-simulated decadal 2 m air temperature (°C) during JJA spanning the terrestrial region of the Atlantic Arctic (60-90°N, 90°W-60°E). Years 0-1270 CE are a part of the past2K run while 1271-1850 CE are from the CESM-LME (Otto-Bliesner et al., 2016). Together, the CESM simulations report similar average coolings to the glacier model results.

Table 1: Plant Radiocarbon Ages

Table 1

Sample # (Fig. 1)	Lab ID	Field ID	Latitude	Longitude	Altitude (m asl)	Distance from 2015 ice margin	^{14}C age (yr)	± (yr)	Calibrated Median Age (yr CE)	1σ Uncertainty (-yr)	1σ Uncertainty (+yr)	2σ Uncertainty (-yr)	2σ Uncertainty (+yr)
1	UCIAMS-167159	M15-B072V	67.15198	-64.82164	1185	0	1005	25	1029	3	33	118	43
2	NSRL-28798	M15-B071V	67.15195	-64.82115	1186	0	1100	15	942	36	41	45	47
3	NSRL-28797	M15-B070V	67.15207	-64.82098	1191	16	1145	15	910	39	28	61	132
4	NSRL-28796	M15-B069V	67.15223	-64.82084	1198	34	1055	15	996	16	9	23	23
5	NSRL-28795	M15-B068V	67.15241	-64.82069	1205	53	880	5	1172	11	13	35	16
6	NSRL-28794	M15-B067V	67.15261	-64.82049	1215	79	770	20	1254	20	24	22	30
7	NSRL-28793	M15-B066V	67.15273	-64.82016	1219	95	505	15	1424	6	7	13	13
8	NSRL-28792	M15-B065V	67.15288	-64.81995	1225	114	380	15	1505	104	50	113	56
9	NSRL-28791	M15-B064V	67.15308	-64.81972	1230	143	310	15	1569	72	45	75	53
10	NSRL-28790	M15-B062V	67.15312	-64.81909	1229	157	1.4933*	0.0025*	1971	8	1	N/A	N/A
11	NSRL-28799	M15-B076V	67.15323	-64.81783	1238	202	175	15	1780	165	111	170	113
12	NSRL-26071	M14-B0170	67.14353	-64.87985	1483	NA	1975	20	26	21	29	29	44

*Sample M15-B062V returned a post-bomb ^{14}C measurement; Fraction modern and uncertainty shown here. Age calculated using OxCal v4.2.4 Bronk and Ramsey (2013) with Post-bomb atmospheric NH1 curve (Hua et al., 2013).